Detecting and Monitoring Artisanal Mining Operations in Semi-Arid Terrain Using Multitemporal SAR Data for InSAR Coherence Estimation and Unsupervised Classification

Ifeanyi Chike[1], Timo Balz[1]

[1]State Key Laboratory of Information Engineering in Surveying, Mapping, and Remote Sensing, Wuhan University, Wuhan 430079, China.- ifybeth1@gmail.com, balz@whu.edu.cn

Keywords: Remote sensing, InSAR, Coherence, PCA, Artisanal mining, Change detection.

Abstract

The impact of artisanal mining in sub-Saharan Africa and other developing countries are often huge as they leave trails of environmental and socio-economic effects on the people and the environment. 123 Multi-temporal SAR data acquired between 2019 and 2023 was used. SARPROZ was used to co-register the images and other preprocessing steps like radiometric and geometric correction to transform the images from SAR coordinates to geographic coordinates after generating all the interferograms. A stack of the 122 coherence map was created. Unsupervised classification was implemented on the stack. Principal component analysis of dimensionality reductions method yielded a far better result than the other unsupervised cluster methods attempted, it showed a very high classification accuracy of the terrain. The principal component analysis worked by computing the covariance matrix of the stacked coherence map then performed eigen-decomposition on it to yield eigenvectors and eigenvalues, The eigenvectors corresponding to the largest eigenvalues represent the principal components. These principal components capture the directions of maximum variance, and the eigenvectors provides a reduced-dimensional representation of the image stack which is then used to reconstruct an approximation of the original image that captures the essential features of the original SAR data. Backscatter intensity of the SAR images processed for this study period for unsupervised change detection and land cover classification, delineated the different features and classes based on long term coherence values.

1. INTRODUCTION

1.1 Background

Artisanal mining, characterized by its informal and small-scale nature, play a key role in various third world economy. It is a means of survival and livelihoods for the teaming populations around the mining communities and their local economy333. However, the environmental consequences of artisanal mining, particularly in terms of land degradation, pose a critical and urgent challenge. For better insight and understanding, we must clearly make that distinction between artisanal mining and other types of mining like large and small-scale mining.

Artisanal system of mining is a type of mining that is purely manual on a small piece of land without any form of mechanization, it involves the use of basic tools such as hand digger, chisel, shovel and head pans. This type of mining is often driven by poverty and the need to survive, the extremely poor people take to this practice to put food on their table.

In contrast the large and small-scale mining is characterized by their mechanized and semi-mechanized nature, they are often carried out on a large scale covering ‘kilometer square area’.

Figure 1. Artisanal mining operation.

Because of the extreme migratory nature of artisanal mining operations where they are seen to rapidly move on from one mine site to a new one tracking and monitoring their operations can be very challenging, especially in areas that are inaccessible due to security challenges. Multi-temporal SAR data was coregistered to match every image pixel by pixel for further processing and coherence generation. Overall, three (3) major remote sensing techniques which includes coherence change detection, unsupervised learning classification, and time-series analysis were combined to detect, classify and visualize the changes occurring over time.

In the review of previous literature, remote sensing has been applied in different ways in the study of various mining related activities.

Ammirati, et al., (Ammirati et al., 2020) in his study applied Differential Interferometric Synthetic Aperture Radar DInSAR technique to monitor surface deformations caused by subsurface artisanal gold mining. Alessi, et al., 2023 (Alessi et al., 2023) is one of the two studies that used SAR images in the study of impact of artisanal mining activities. However, in their study they only attempted to detect the river dredging machine used in the dredging of the river for alluvial gold deposit where they adopted a fairly straight-forward techniques of search for unidentified marine objects (SUMO).

In the paper ‘Mine detection experiments using hyperspectral sensors’ authored by Winter, et al.(Winter et al., 2004) focuses on the application of hyperspectral imaging technology for the detection of surface and buried land mines. Wang, et al.(Wang et al., 2013) in their publication ‘Application of remote sensing for investigating mining geological hazards’ adopted a unique method where the vegetation was substituted first through the use of the normalized difference vegetation index on the GeoEye-1 data. Wu, et al.(Wu et al., 2018) in ‘Remote sensing detection of vegetation and landform damages by coal mining on the Tibetan plateau’ proposed an automated method that detects the timing of the inception of mining development & then assesses the spatial

distribution of destroyed vegetation covers resulting from mining operations.

Other related studies largely focused on the environmental impact of artisanal mining. Ako et al., 2014 (Ako et al., 2014) on this study titled ‘Environmental Impact of Artisanal Gold Mining in Luku’ focus was on the gold mining activities and the various level of impact it has on the host community Luku, Niger State, Nigeria. Elvis Munyoka, 2020 (Elvis Munyoka, 2020), In the study ‘Mining and Environmental Rights in Zimbabwe. A Case of Zvishavane District’, highlights the effects of artisanal & small-scale mining operations on our environment. The study reveals that these activities have led to excessive land distortion, deforestation, water pollution, as well as air quality pollution, exposing mining communities to health problems like cholera outbreaks, bilharzia, triggers to asthma attacks, and cirrhosis. Donkor et al., 2009 (Donkor et al., 2009) in the paper ‘Artisanal Mining of Gold with Mercury in Ghana’, delves deeply into the overall impact of artisanal gold mining on the environment, drawing attention to its contribution of land degradation, unmitigated biodiversity loss, deforestation, and pollution of water bodies. Otamonga & Poté, 2020 (Otamonga and Poté, 2020) explores the environmental and socio-economic problems that comes with abandoned mines and Artisanal & small-scale Mining (ASM) in the Democratic Republic of Congo (DRC). The review delves into the impacts on public health and the surrounding environment.

1.2 Study area

The study area is a square area, a little over 1000 square kilometers littered with so much artisanal gold mining sites. The terrain is mostly semi-arid, and largely influenced by the predominant two seasons that prevails in Nigeria. The harmattan which is the dry season starts from November to March and is usually accompanied with heavy dry dust. The Zamfara state temperature ranges between 35^0c to 40^0c degree and is divided into different Savannah; Sahel, Arid and Guinea (Nwabueze Chukwuji et al., 2019).

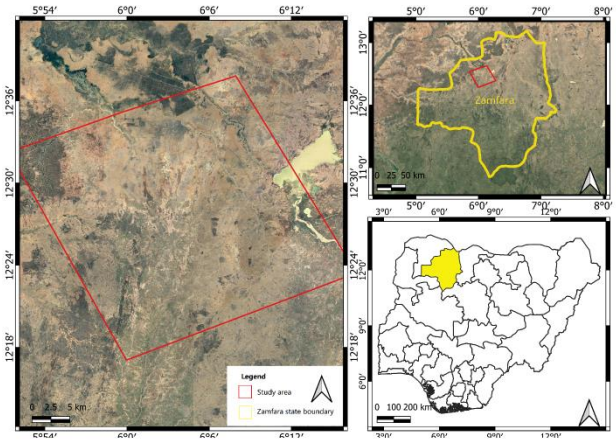

Figure 2.Map showing the study area.

2. MATERIALS AND METHOD

2.1 Data collection

In order to conduct a comprehensive analysis of land surface changes over time in order to detect and perform classification Sentinel-1A Synthetic Aperture Radar (SAR) data was chosen for its ability to penetrate clouds and provide high-resolution imagery. The Sentinel-1A data used in this study was obtained from the European Space Agency's (ESA) Copernicus Open Access Hub

The Sentinel-1A SAR data used in this study offers a 12-day revisit interval and covers the entire study area. This temporal resolution is deemed appropriate for capturing frequent changes in land cover and land use associated with artisanal gold mining activities. access to Sentinel-1A SAR data was facilitated through the Copernicus Data Space Ecosystem https://dataspace.copernicus.eu, following standard procedures outlined by the European Space Agency. The acquired Sentinel-1A SAR data is characterized by both VH and VV polarization, high spatial resolution. These characteristics were considered optimal for the objectives of this study, ensuring the detection of subtle changes in the landscape associated with artisanal gold mining.

Table 1. Acquisition parameters

Product	*Date*	*Product description*
Sentinel 1A	April 2019	Satellite: sentinel-1A
		Instrument: SAR (C-band)
		Mode: IW
		Pass: Ascending
		Polarization: VV, VH
		Relative orbit: 30
		Slice number: 9
	May 2023	Product type: SLC

2.2 Method

This section systematically highlights the series of steps and workflow involved in this study.

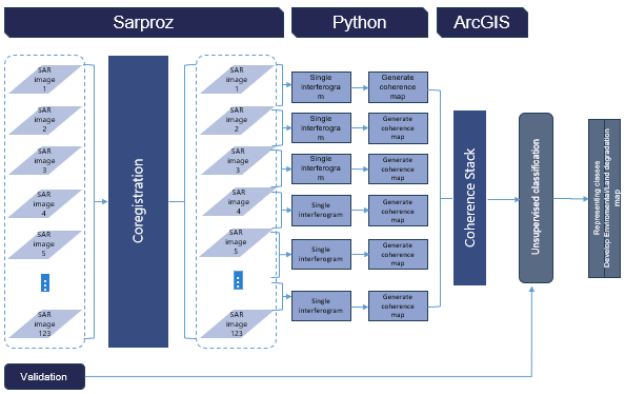

Figure 3.workflow: schematic display of the input-output process for the study

2.2.1 Coregistration

Coregistration refers to the process of aligning multiple SAR images spatially so that corresponding features in the scenes overlap accurately. By aligning SAR images through coregistration, we can eliminate any geometric distortions and ensure accurate analysis of the data. In the field of Interferometric Synthetic Aperture Radar, accurate coregistration of SAR image pairs is crucial for generating coherent interferograms and digital elevation models (Mao et al., 2009). it ensures accurate spatial alignment of images and improves the coherence and precision of the analysis, leading to more reliable and meaningful results in various applications (Wen et al., 2010). This process is expressed.

$$\begin{bmatrix} x_i^{\dagger} \\ y_i^{\dagger} \\ 1 \end{bmatrix} = \begin{bmatrix} a_{1i} & b_{1i} & c_{1i} \\ a_{2i} & b_{2i} & c_{2i} \\ 0 & 0 & 1 \end{bmatrix} \begin{bmatrix} x_i \\ y_i \\ 1 \end{bmatrix}$$

where,

a_{1i} *and* a_{2i} *are scaling f actors f or the x – coordinate*

b_{1i} *and* b_{2i} *are scaling f actors f or the x – coordinate*

c_{1i} *and* c_{2i} *are translation parameters specif ic to the transf ormation f rom the coordinate system of* I_1 *to* I_i

(1)

The matrix $\begin{bmatrix} a_{1i} & b_{1i} & c_{1i} \\ a_{2i} & b_{2i} & c_{2i} \\ 0 & 0 & 1 \end{bmatrix}$ *represents the transf ormation matrix f or the i – th image (in this case the 123rd image)*

To represent the overall transf ormation f rom the f irst SAR image (I_1) *to the 123rd image* (I_i) *in matrix f orm*

$$\begin{bmatrix} x_i^{\dagger} \\ y_i^{\dagger} \\ 1 \end{bmatrix} = \begin{bmatrix} a_{11} & b_{11} & c_{11} \\ a_{21} & b_{21} & c_{21} \\ 0 & 0 & 1 \end{bmatrix} \begin{bmatrix} a_{12} & b_{12} & c_{12} \\ a_{22} & b_{22} & c_{22} \\ 0 & 0 & 1 \end{bmatrix} \cdots\cdots \begin{bmatrix} a_{1i} & b_{1i} & c_{1i} \\ a_{2i} & b_{2i} & c_{2i} \\ 0 & 0 & 1 \end{bmatrix} \begin{bmatrix} x_i \\ y_i \\ 1 \end{bmatrix}$$

This shows the cummulative transf ormation f rom the coordinate system of I_1 *to* I_i

2.2.2 Geometric calibration

This process involves aligning the radar imagery with precise georeferencing data, such as a digital elevation model and ground control points. By accurately calibrating the SAR image to a common radar coordinate system, the resulting data can be effectively utilized for various applications, including measuring and mapping terrain, monitoring slope deformations, and generating digital elevation models. Geometric calibration ensures that the SAR images are aligned with accurate georeferencing data, allowing for precise measurements and mapping of terrain.

2.2.3 Radiometric calibration

Transforming the digital numbers (DN) or radiance values in the image to physical units, typically reflectance or radiance at the sensor level. The goal is to convert the raw digital values into meaningful, standardized values that can be used for quantitative analysis. It ensures that the pixel values in the image accurately represent the backscatter intensity of the radar signal. This is because the raw pixel values captured by the SAR instrument may be influenced by various factors such as sensor gain, antenna pattern, and other system-specific characteristics.

2.2.4 Interferogram generation

This step involves analysing the phase differences between multiple radar images to generate an interferogram. This interferogram provides information about ground surface deformation, such as changes in elevation or displacement. To generate an interferogram, two complex SAR images of the same area are acquired from slightly different look angles (Wang et al., 2011).

2.2.5 Coherence

In SAR interferometry coherence is the temporal stability and correlation of the phase information between two or more SAR images acquired at different times. Coherence is a critical parameter because it directly affects the accuracy and reliability of the interferometric phase, which is used to derive deformation information, so it is the measure of the correlation between the complex values of two SAR images which ranges from 0 to 1, where 0 represents no correlation and 1 represents perfect correlation. Two waves with a phase difference that remains constant over time are said to be coherent (Washaya et al., 2018), therefore, Coherence is thus defined as the amplitude of the complex correlation coefficient between two SAR images. The coherence is estimated on a given window size, using the equation below.

$$\gamma = \left| \frac{\frac{1}{N}\sum_{i=0}^{N} M_i S_i^*}{\sqrt{\frac{1}{N}\sum_{i=0}^{N} M_i M_i^* \frac{1}{N}\sum_{i=0}^{N} S_i S_i^*}} \right| \qquad (2)$$

where

γ = resulting coherence
N = the number of neighbouring pixels to be estimated
M = the complex master image
S = the complex slave image
* denotes the complex conjugate (Washaya et al., 2018).

2.2.6 Principle component analysis

Principal Component Analysis (PCA) is a versatile technique in satellite image processing and computer vision, providing a means to reduce the dimensionality of high-dimensional satellite data while preserving critical information. This dimensionality reduction is particularly beneficial for tasks such as feature extraction, noise reduction, and efficient representation of satellite imagery. The covariance matrix C is given by:

$$C = \frac{1}{m-1}(X - \bar{X})^{T}(X - \bar{X}) \qquad (3)$$

The eigenvectors corresponding to the largest eigenvalues represent the principal components. These principal components capture the directions of maximum variance in the satellite image data. The transformed data *Y* can be obtained by projecting the original data onto the space defined by the principal components:

$$Y = (X - \bar{X}) \cdot V_k \qquad (4)$$

The reduced-dimensional representation Y can be used to reconstruct an approximation of the original image. This is achieved by multiplying *Y* by the transpose of V_k and adding back the mean $\bar{X}$

$$X_{reconstructed} = Y.V_k^T + \bar{X} \qquad (5)$$

3. RESULTS

3.1 Coherence change detection

Coherence maps were generated from the interferograms with a small temporal baseline which in essence means that they were generated using SAR images acquired within close time interval. For this study, we used 12 days temporal baseline spanning 5 years period, a time range between 2019 and 2023. In total, 122 coherence maps were generated from the 123 SAR images

acquired and they had varying coherence which can be linked to the time of the year the images were acquired and the prevailing season at the time of acquisition. In Nigeria, there are two prevailing seasons, the rainy season which starts in April and ends in October. The dry season is between November and March. Generally, it can be noticed that the coherence maps generated from images acquired during the dry season had a brighter reflectance compared to the ones from the rainy season.

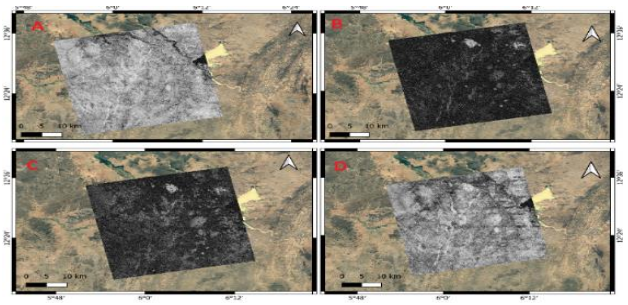

Figure 4. Coherence maps generated from both rainy and dry season. Maps A (between Jan. & Mar) and D (between Nov & Dec) were both generated within the dry season window, while B & D were generated Apr and Oct within the rainy season window.

Observable pattern when scrutinizing the distinctive characteristics of reflectance of the 122 coherence maps was the pattern repetition seen occurring every year within the study period where coherence maps emanating from images procured during the dry season manifest a discernibly heightened reflectance when compared against their counterparts derived from imagery acquired during the rainy season after methodically synthesized datasets collected between 2019& 2023 while adhering to a consistent temporal baseline of 12 days (figure 4).

3.2 Image stack

Stack consisting of 122 coherence maps was generated by arranging each coherence map as a separate band within the new stack. This stacking process was accomplished using the image analysis tool available in the ArcGIS software. Essentially, each coherence map was treated as a distinct layer, and by leveraging the capabilities of ArcGIS, they were systematically combined to form a cohesive stack, facilitating further analysis and visualization of the data. (see figure 5)

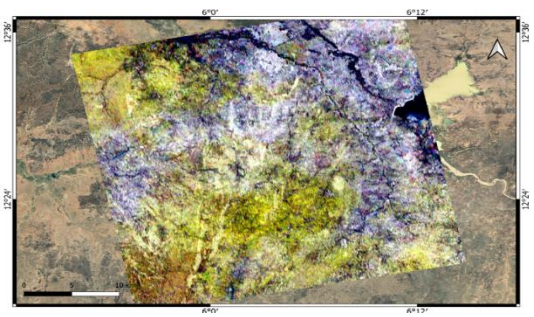

Figure 5. Coherence stack of 122 maps.

3.3 Principal Component Analysis

Principal Component Analysis (PCA) was used to delineate distinct representative classes within the dataset. Four primary classes emerged from this analytical process, each contributing valuable insights into the features present within the study area (see figure 6). The first class pertains to brightly scattering settlements, discerned and highlighted in vibrant red hues on the resulting classification map. This category encapsulates areas characterized by intense backscattering signals, typically indicative of human settlements. The second class is attributed to mine sites, meticulously classified and distinguished by a flesh pink coloration on the map. This specific classification enables the identification and differentiation of areas associated with artisanal mining activities, providing valuable information for land degradation and environment. The third class is characterized by a sky bluish green appearance on the classification map, signifying vegetated areas. This class encompasses regions with healthy vegetation cover, and the distinct coloration aids in differentiating these areas from other land cover types. The fourth and final class is denoted by a deep blue coloration, which designates low-coherent water bodies.

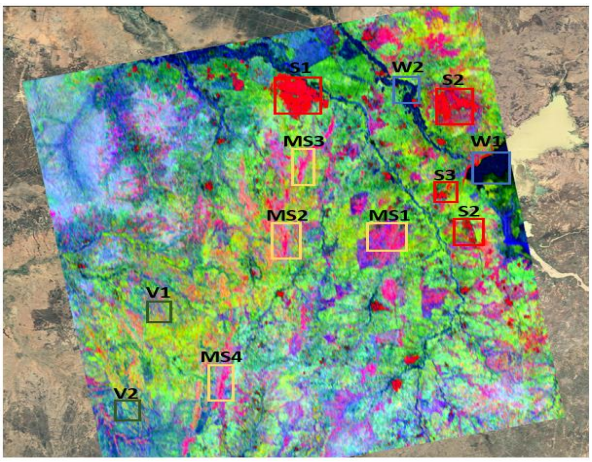

Figure 5. The four (4) representative classes for at least two different locations for each class. Where S= settlement, MS= mine site, W= water and V= vegetation

3.4 Validation: The result of this study was validated against both small-scale mining lease and exploration licenses shapefiles (.shp data) from the Mining cadastre office of the Ministry of Mines and Steel Development Nigeria and over 90% of the classified mine sites fell under these lease polygons covering mineral titles of gold mining (see figure 7).

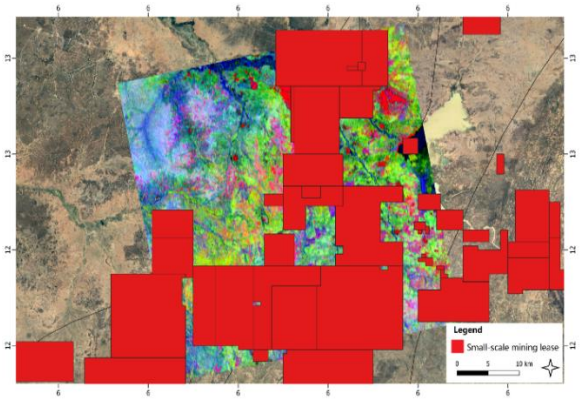

Figure 7. Validation map

Further validation was done on the representative classes, all the selected classes and sites in this study were compared to the specific location on a zoomed in image of google earth using their geographic coordinates to further ascertain the accuracy of the unsupervised classification. As can be seen from the picture merge of various locations or points from the result and their corresponding location on google earth image, which is correlated with their geographic coordinates, the result showed a very high classification accuracy (see figure 8 & 9).

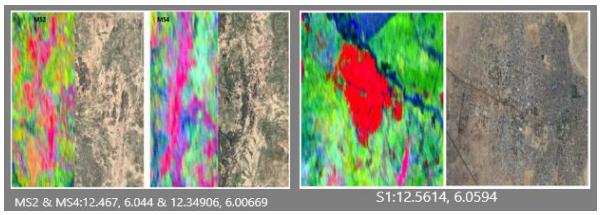

Figure 8. Correlation of MS1, MS4 and S1 with high-resolution optical image.

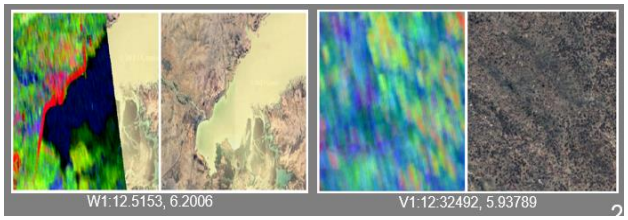

Figure 9. Correlation of W1 and V1 with high resolution optical image.

4. DISCUSSION

Between April 2019 and May 2023, a total of 122 coherence maps of the study area was generated from 123 multitemporal SAR images with short temporal baseline of 12 days. This allowed for selecting multiple-master InSAR images, pairing two at a time, usually denoted by short temporal as well as spatial baselines, this then preserved the coherence while also enabling the retrieval of important information on the phase history of the interferograms (Pepe, 2021) as opposed to creating a ‘star network’ pairing in which all the images are paired and coregistered to a single master which is usually more effective in built up areas and would require a dominant permanent scatterer, it was bound to be affected by decorrelation in this study area because it identifies pixels primarily based on their phase variation in time(Hooper, 2008). The coherence result showed a variation of backscatter intensity in which the maps generated between November and April every year backscatter brightly while those between May and October appears darker between of lower backscatter intensity. These two windows correlate with the two season that is prevalent in Nigeria. The rainy season window which falls between May and October plays a major role as the rains could be a major decorrelation factor thereby causing low back scatter hence the darker coherence maps. Decorrelation which is the reduction of InSAR coherence with change in surface scattering properties due to vegetation or precipitation (Agram and Simons, 2015). During the dry season, the study area is usually bare or sparsely vegetated. Therefore, high interferometric correlation is observed during this time period (Wegmiiller’ and Werner2, n.d.).

The implementation of unsupervised learning algorithm to the stack of all (122) the coherence maps was done to classify and visualize the distinct landcover class in order to separate areas that are vegetated, artisanal mines sites, settlements and water bodies. Through the unsupervised learning technique, information from the stacked multitemporal coherence maps are used to obtain the distinguishable land cover classes (Aswatha et al., 2020)

Principal component analysis of Dimensionality reductions method yielded a good result which showed a very high classification accuracy of the terrain. The principal component analysis works by computing the covariance matrix of the stacked SAR data then performed eigen-decomposition on it to yield eigenvectors and eigenvalues, The eigenvectors corresponding to the largest eigenvalues represent the principal components. The purpose is to retrieve the key information from the table, to represent it as a set of new orthogonal variables called principal components (Abdi and Williams, 2010) These principal components capture the directions of maximum variance and the eigenvectors provides a reduced-dimensional representation of the image stack which is then used to recreate a close reference of the original image that captures the essential features of the original SAR data while reducing noise and redundant information. Shows the similarity trend of the observations and of the variables as points in maps (Abdi and Williams, 2010). This unsupervised learning technique was able to accurately distinguish all the landcover classes in figure 30, all the settlements or nearby hamlets were all represented with deep red cluster, while the artisanal mine sites that are spread all around the area of study is shown with the flesh pink coloration, the vegetation and water bodies are represented with green and blue respectively. These flesh pink coloration patches all over the classification map are the detected mines sites, it is a visual representation of land degradation within the square area of study (see figure 30).

5. CONCLUSION

Two (2) different techniques were uniquely combined and implemented to remotely detect and classify landcover in the study area leveraging on the temporal changes caused by the rapidly changing artisanal mining operations. The two techniques adopted was InSAR coherence change detection and unsupervised learning technique. It helped gain an insightful knowledge on how to remotely detect and track these activities in sub-saharan Africa which is majorly semi-arid in nature. For unique landscape like the semi-arid northern Nigeria, the unsupervised classification method principal component analysis PCA has proven to be very effective with a very high accuracy.

6. REFERENCES

Abdi, H., Williams, L.J., 2010. Principal component analysis. Wiley Interdiscip Rev Comput Stat. https://doi.org/10.1002/wics.101

Agram, P.S., Simons, M., 2015. A noise model for InSAR time series. J Geophys Res Solid Earth 120, 2752–2771. https://doi.org/10.1002/2014JB011271

Ako, T.A., Onoduku, U.S., Oke, S.A., Adamu, I.A., Ali, S.E., Mamodu, A., Ibrahim, A.T., 2014. Environmental Impact of Artisanal Gold Mining in Luku, Minna, Niger State, North-Central Nigeria. Journal of Geosciences and Geomatics 2.

Alessi, M.A., Chirico, P.G., Millones, M., 2023. Artisanal Mining River Dredge Detection Using SAR: A Method Comparison. Remote Sens (Basel) 15. https://doi.org/10.3390/rs15245701

Ammirati, L., Mondillo, N., Rodas, R.A., Sellers, C., Martire, D. Di, 2020. Monitoring land surface deformation associated with gold artisanal mining in the Zaruma City (Ecuador). Remote Sens (Basel) 12. https://doi.org/10.3390/rs12132135

Aswatha, S.M., Mukherjee, J., Biswas, P.K., Aikat, S., 2020. Unsupervised classification of land cover using multi-modal data from multi-spectral and hybrid-polarimetric SAR imageries. Int J Remote Sens 41, 5277–5304. https://doi.org/10.1080/01431161.2020.1731771

Donkor, A., Nartey, V., Bonzongo, J., Adotey, D., 2009. Artisanal mining of gold with mercury in Ghana. West African Journal of Applied Ecology 9. https://doi.org/10.4314/wajae.v9i1.45666

Elvis Munyoka, 2020. Mining and Environmental Rights in Zimbabwe. A Case of Zvishavane District. Developing Country Studies. https://doi.org/10.7176/dcs/10-8-06

Hooper, A.J., 2008. A multi-temporal InSAR method incorporating both persistent scatterer and small baseline approaches. Geophys Res Lett 35. https://doi.org/10.1029/2008GL034654

Mao, Z.J., Liao, G.S., Yang, Z.W., 2009. Image auto-coregistration and InSAR interferometric phase estimation based on optimum data vector. Xitong Fangzhen Xuebao / Journal of System Simulation 21.

Nwabueze Chukwuji, C., Gadanga Tsafe, A., Yusuf, Z., Zakariya, afar, Nwabueze, C., Gadanga, A., Chukwuji, B., 2019. Awareness, Access and Utilization of Information on Climate Change by Farmers in Zamfara State, Nigeria Part of the Library and Information Science Commons Awareness, Access and Utilization of Information on Climate Change by Farmers In Zamfara State, Nigeria.

Otamonga, J.P., Poté, J.W., 2020. Abandoned mines and artisanal and small-scale mining in Democratic Republic of the Congo (DRC): Survey and agenda for future research. J Geochem Explor. https://doi.org/10.1016/j.gexplo.2019.106394

Pepe, A., 2021. Multi-temporal small baseline interferometric sar algorithms: Error budget and theoretical performance. Remote Sens (Basel) 13, 1–28. https://doi.org/10.3390/rs13040557

Wang, Q., Guo, H., Chen, Y., Lin, Q., Li, H., 2013. Application of remote sensing for investigating mining geological hazards. Int J Digit Earth 6, 449–468. https://doi.org/10.1080/17538947.2011.629009

Wang, Y., Wu, T., Zhan, J., Ge, J., Jiang, K., 2011. System design and experimental results of polarimetric SAR interferometry, in: Proceedings of 2011 IEEE CIE International Conference on Radar, RADAR 2011. https://doi.org/10.1109/CIE-Radar.2011.6159464

Washaya, P., Balz, T., Mohamadi, B., 2018. Coherence change-detection with Sentinel-1 for natural and anthropogenic disaster monitoring in urban areas. Remote Sens (Basel) 10. https://doi.org/10.3390/rs10071026

Wegmiiller’, U., Werner2, C.L., n.d. Farmland monitoring with SAR interferometry.

Wen, J., Liao, G.S., Zhu, S.Q., 2010. Method for ground moving target indication and velocity estimation based on InSAR system. Xi Tong Gong Cheng Yu Dian Zi Ji Shu/Systems Engineering and Electronics 32.

Winter, E.M., Miller, M.A., Simi, C.G., Hill, A.B., Williams, T.J., Hampton, D., Wood, M., Zadnick, J., Sviland, M.D., 2004. Mine detection experiments using hyperspectral sensors, in: Detection and Remediation Technologies for Mines and Minelike Targets IX. SPIE, p. 1035. https://doi.org/10.1117/12.548087

Wu, Q., Liu, K., Song, C., Wang, J., Ke, L., Ma, R., Zhang, W., Pan, H., Deng, X., 2018. Remote sensing detection of vegetation and landform damages by coal mining on the Tibetan Plateau. Sustainability (Switzerland) 10. https://doi.org/10.3390/su10113851